processes

MDPI

Article

In Situ Formation of Titanium Diboride/Magnesium Titanate Composites by Magnesiothermic-Based Combustion Synthesis

Chun-Liang Yeh * and Chen Chen

Department of Aerospace and Systems Engineering, Feng Chia University, Taichung 407102, Taiwan; hayama6318@gmail.com

* Correspondence: clyeh@fcu.edu.tw; Tel.: +88-64-2451-7250 (ext. 3963)

Abstract: In situ formation of TiB_2–Mg_2TiO_4 composites was investigated by combustion synthesis involving the solid-state reaction of Ti with boron and magnesiothermic reduction of B_2O_3. Certain amounts of MgO and TiO_2 were added to the reactant mixtures of Ti/B/Mg/B_2O_3 to act as the moderator of highly exothermic combustion and a portion of the precursors to form Mg_2TiO_4. Two combustion systems were designed to ensure that synthesis reactions were sufficiently energetic to carry on self-sustainably, that is, in the mode of self-propagating high-temperature synthesis (SHS). Consistent with thermodynamic analyses, experimental results indicated that the increase in pre-added MgO and TiO_2 decreased the combustion temperature and propagation velocity of the flame front. MgO was shown to have a stronger dilution effect on combustion exothermicity than TiO_2, because the extent of magnesiothermic reduction of B_2O_3 was reduced in the MgO-added samples. In situ formation of the TiB_2–Mg_2TiO_4 composite was achieved from both types of samples. It is believed that, in the course of the SHS progression, Mg_2TiO_4 was produced through a combination reaction between MgO and TiO_2, both of which were entirely or partially generated from the metallothermic reduction of B_2O_3. The microstructure of the products exhibited fine TiB_2 crystals in the shape of short rods and thin platelets that existed within the gaps of Mg_2AlO_4 grains. Both constituent phases were well distributed. A novel and efficient synthesis route, which is energy- and time-saving, for producing Mg_2TiO_4-containing composites was demonstrated.

Keywords: Mg_2TiO_4; TiB_2; magnesiothermic reduction; combustion synthesis; reaction exothermicity

check for updates

Citation: Yeh, C.-L.; Chen, C. In Situ Formation of Titanium Diboride/Magnesium Titanate Composites by Magnesiothermic-Based Combustion Synthesis. *Processes* **2024**, *12*, 459. https://doi.org/10.3390/pr12030459

Academic Editors: Andrey Yurkov, Denis Kuznetsov and Maria Vartanyan

Received: 4 February 2024
Revised: 16 February 2024
Accepted: 22 February 2024
Published: 24 February 2024

1. Introduction

Titanium diboride (TiB_2), belonging to the family of ultra-high temperature ceramics (UHTCs) [1–3], possesses a high melting point, low density, metallic electrical conductivity, good thermal stability, excellent wear resistance, corrosion and oxidation resistance, and thermal shock resistance [3,4]. Such a unique combination of material properties renders TiB_2 suitable for applications in molten metal crucibles, cutting tools, wear resistance parts, high-temperature structural components, cathodes for alumina smelting, ballistic armors, rocket nozzles, etc. [3–6]. Moreover, TiB_2 has received increasing attention for use as a high-temperature microwave-absorbing material recently on account of its high electrical conductivity, great thermal stability, and outstanding resistance to harsh conditions [3]. Many TiB_2-based ceramics, such as TiB_2/MgO, TiB_2/Al_2O_3, TiB_2/SiC, and TiB_2/Al_2O_3/$MgAl_2O_4$ composites, were recognized for their excellence in high-temperature microwave absorption and dielectric properties [7–11]. Magnesium titanate spinel, Mg_2TiO_4, is particularly renowned for its microwave dielectric properties [12,13], which motivates the fabrication of an innovative composite composed of TiB_2 and Mg_2TiO_4. When compared with their constituent components, TiB_2–Mg_2TiO_4 composites enhance the microwave absorption and dielectric properties of TiB_2 and increase the corrosion, oxidation, and thermal shock resistances of Mg_2TiO_4. It is significant to develop the TiB_2–Mg_2TiO_4 composite as a new refractory material for microwave-tunable devices, voltage-controlled oscillators, dielectric substrates, phase shifters, filters, and antennas to be utilized in harsh environments [12–15].

There are three stable magnesium titanates ($MgTiO_3$, Mg_2TiO_4, and $MgTi_2O_5$) in the $MgO–TiO_2$ system. Two of them, $MgTiO_3$ and Mg_2TiO_4, exhibit excellent microwave dielectric properties [14], and especially, there is a growing interest in developing Mg_2TiO_4-based composites as a novel microwave dielectric material [14–19]. Conventionally, Mg_2TiO_4 has been fabricated by the solid-state reaction between TiO_2 and MgO under elevated temperatures of 1300–1500 °C for 4–6 h [15–18]. Cheng et al. [14] prepared Mg_2TiO_4 with MgO and TiO_2 by high-energy ball milling for 30 h, and nanosized Mg_2TiO_4 powders were synthesized at 1000 °C, about 300 °C lower than that by a conventional solid-state reaction process. Composite-type Mg_2TiO_4-$MgTiO_3$ ceramics were produced by the solid-phase sintering of TiO_2 and MgO powders at 1290–1410 °C for 2–8 h [15]. Solid solutions of $MgAl_2O_4$-Mg_2TiO_4 spinel ceramics were obtained by the solid-state reaction at 1350–1450 °C for 4 h [18]. Zhang et al. [19] prepared Mg_2TiO_4-based composite ceramics by the hydrothermal method. After removing the solvent and binder at 550 °C for 6 h, Mg_2TiO_4 was synthesized at sintering temperatures below 1300 °C.

As a potential alternative, self-propagating high-temperature synthesis (SHS) or combustion synthesis capitalizes on highly exothermic reactions and is efficient and economical in time, energy, and costs [20,21]. When a traditional SHS process combines with metallothermic reduction of oxide compounds, this composite type of synthesis scheme symbolizes an in situ production route to prepare composite materials containing Al_2O_3 and magnesium aluminate spinel ($MgAl_2O_4$) [22–27]. For example, the aluminothermic reduction of WO_3 and B_2O_3 was incorporated with SHS to prepare Al_2O_3-WSi_2-WB_2-WB composites [22]. TiB_2-Al_2O_3 and NbB_2-Al_2O_3 composites were produced via an aluminothermic-based SHS technique with reactant mixtures containing Al-TiO_2-B_2O_3 and Al-Nb_2O_5-B_2O_3, respectively [23]. $MgAl_2O_4$-based composites with $MoSi_2$ and Mo_5Si_3 were produced by the SHS process involving co-reduction of SiO_2 and MoO_3 by Al in the presence of MgO [24]. Composite materials of $MoSi_2$ and $MgAl_2O_4$ were also synthesized by incorporating the metallothermic reduction of MoO_3 by Al and Mg as dual reducing agents into the Mo–Si combustion system [25]. The addition of MgO into a reactant mixture consisting of TiO_2, B_2O_3, and Al was applied to prepare TiB_2–$MgAl_2O_4$ composites through a reduction-based combustion process [26]. A recent study on the synthesis of TiB_2–$MgAl_2O_4$ composites via SHS indicated that $MgAl_2O_4$ was produced by a combination reaction between MgO and Al_2O_3, both of which were partially or entirely generated from co-reduction of TiO_2 and B_2O_3 by Al and Mg [27]. Magnesium titanate Mg_2TiO_4 refers to an inverse spinel compound and has the same spinel structure and space group as $MgAl_2O_4$ [18]. Nonetheless, there are no studies on the combustion synthesis of Mg_2TiO_4-based composites in the available literature.

This study made the first effort to investigate the fabrication of TiB_2–Mg_2TiO_4 composites by metallothermic and self-sustaining combustion synthesis, within which magnesiothermic reduction of B_2O_3 was integrated with solid-state combustion between Ti and boron in the presence of MgO and TiO_2. The role of pre-added MgO and TiO_2 was explored as a combustion moderator and precursor of Mg_2TiO_4. The exothermicity of the SHS reaction, referring to the enthalpy of the reaction and adiabatic combustion temperature, was evaluated. The combustion wave kinetics of the SHS reaction were examined by measuring the combustion front velocity and temperature, and the activation energy of the reaction was deduced. The composition and microstructure of the synthesized products were analyzed.

2. Materials and Methods

This study utilized the following oxide and elemental compounds as the reactants, including MgO (Acros Organics, Mount Olive, NJ, USA, 99.5%), TiO_2 (Acros Organics, Mount Olive, NJ, USA, 99.5%), Mg (Alfa Aesar, Ward Hill, MA, USA, <45 μm, 99.8%), B_2O_3 (Acros Organics, Mount Olive, NJ, USA, 99%), amorphous boron (B) (Noah Technologies, San Antonio, TX, USA, <1 μm, 93.5%), and Ti (Alfa Aesar, Ward Hill, MA, USA, <45 μm,

99.8%). Two reaction systems were designed and formulated as Equations (1) and (2) for the synthesis of $1.5TiB_2 + Mg_2TiO_4$ composites.

$$\left(\frac{4-x}{3}\right)B_2O_3 + (2-x)Mg + xMgO + \frac{5}{2}Ti + \left(\frac{1+2x}{3}\right)B \rightarrow 1.5TiB_2 + Mg_2TiO_4 \quad (1)$$

$$\left(\frac{4-2y}{3}\right)B_2O_3 + 2Mg + yTiO_2 + \left(\frac{5-2y}{2}\right)Ti + \left(\frac{1+4y}{3}\right)B \rightarrow 1.5TiB_2 + Mg_2TiO_4 \quad (2)$$

where x and y are stoichiometric coefficients indicating the number of moles of MgO and TiO_2 in the green mixtures of the reaction system (1) and (2), respectively. To ensure a self-sustaining process, the reaction system (1) was conducted with $0.1 \leq x \leq 1.0$ and (2) with $0.1 \leq y \leq 1.0$ in this study.

The metallothermic reagents of both combustion systems comprised B_2O_3 as the oxidant and Mg as the reducing agent. Ti and boron powders were adopted for the production of TiB_2. Pre-added MgO and TiO_2 not only acted as a combustion diluent to moderate the highly exothermic reactions, but they also constituted a part of the precursors for the formation of Mg_2TiO_4. The other part of MgO and TiO_2 required for the synthesis of Mg_2TiO_4 was supplied from metallothermic reduction reactions.

The combustion exothermicity of the reaction systems (1) and (2) was investigated by first calculating the enthalpy of reaction (ΔH_r) at 298 K and, second, by evaluating the adiabatic combustion temperature (T_{ad}) under different stoichiometric coefficients of x and y. Equation (3) was the energy balance equation [26,27] for computing T_{ad}, and the required thermochemical data were taken from [28].

$$\Delta H_r + \int_{298}^{T_{ad}} \sum n_j c_p(P_j) dT + \sum_{298-T_{ad}} n_j L(P_j) = 0 \quad (3)$$

where n_j is the stoichiometric coefficient of the product (i.e., n_j = 1.5 for TiB_2 and n_j = 1.0 for Mg_2TiO_4 in this study), $c_p(P_j)$ is the specific heat of the product, and $L(P_j)$ is the latent heat of the product.

The well-mixing of dry reactant powders was accomplished by a tumbler ball mill. Reactant powders and alumina grinding balls of 2.5 mm in diameter were contained in a glass cylindrical bottle that rotated about its longitudinal axis. The tumbler ball mill operated at 90 rpm, and the milling time was 4 h. Then, the blended powders were uniaxially compressed in a stainless-steel mold under a packing pressure of 70–80 MPa to prepare test specimens with a height of 12 mm, a diameter of 7 mm, and a relative density of 55%. The SHS experiments were performed in a windowed combustion chamber. The chamber was first purged with high-purity (99.99%) argon for 3 min and then filled with argon at 0.25 MPa. A schematic diagram of the experimental setup [29] is shown in Figure 1. The ignition of the powder compact was achieved by a heated tungsten coil with a voltage of 120 V and a current of 5 A. Based on the time series of recorded combustion images, the propagation velocity of the self-sustaining combustion wave (V_f) was determined from the time derivative of the combustion front trajectory. The exposure time of each recorded image was set at 0.1 ms. A beam splitter with a mirror characteristic of 75% transmission and 25% reflection was used to optically superimpose a scale onto the image of the sample in order to accurately measure the instantaneous locations of the combustion front. The location of the combustion front in each recorded photo was determined by the variation in the gray-level number of pixels. The IMAQ Vision for LabVIEW software (version 6.1) was used to identify the position with the largest directional derivative, which is considered the location of the combustion front. The trajectory of the combustion front was then constructed by plotting the position versus time, and the derivative of position with respect to time was the combustion front velocity.

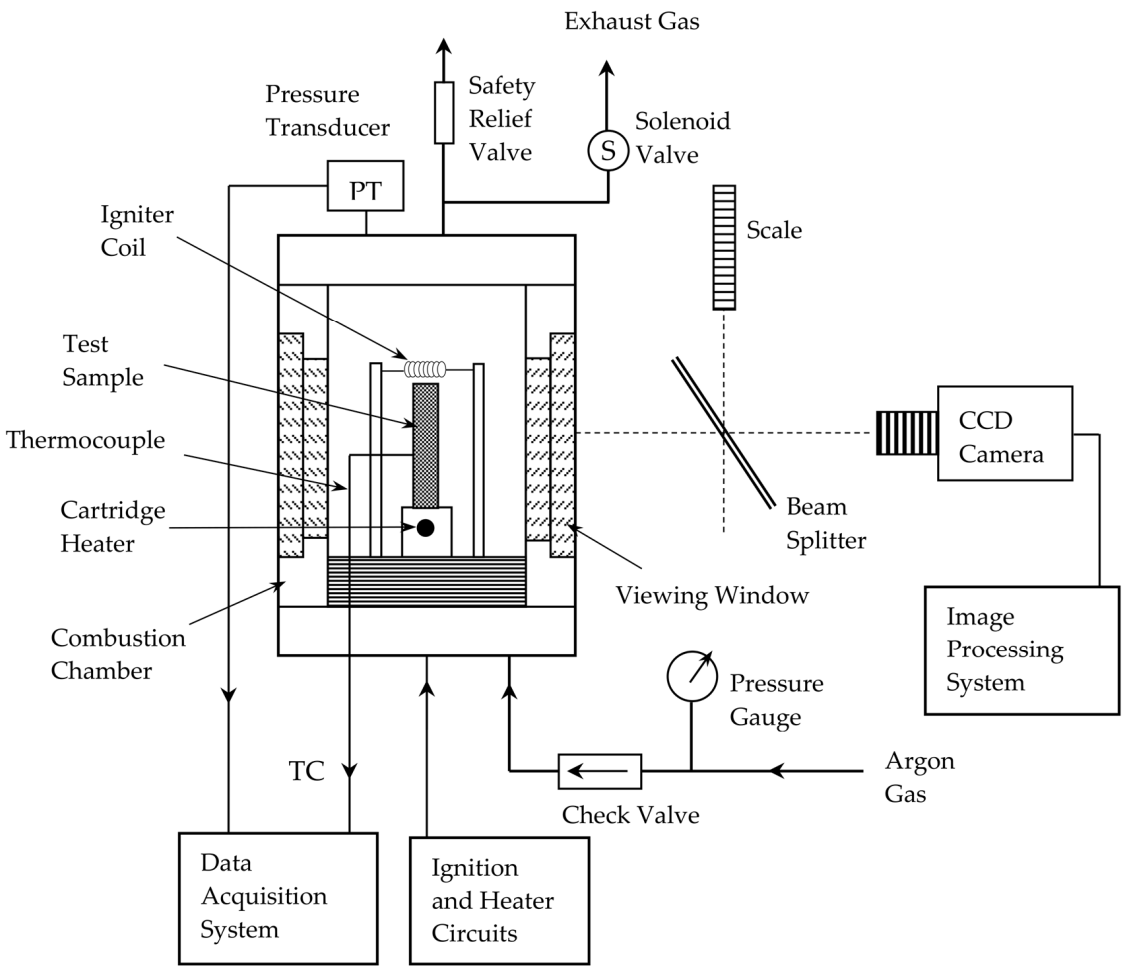

Figure 1. Schematic diagram of experimental setup for combustion synthesis of TiB_2–Mg_2TiO_4 composites.

The combustion temperature was measured by a bare Pt/Pt-13%Rh (R-type) thermocouple with a bead diameter of 125 µm, and the thermocouple was mounted at a position about 6–7 mm from the ignited top plane of the sample. For the synthesized products, the phase composition was identified by a Bruker D2 X-ray diffractometer (XRD Phaser, Karlsruhe, Germany). The diffractometer features a high-precision theta–theta goniometer and uses CuK_α radiation with wavelength λ = 1.5406 Å. The range of the scan was 20°–80° with a scanning rate of 0.05°/s. The microstructure and elemental analysis of the final products were examined by scanning electron microscopy (Hitachi S3000H, Tokyo, Japan) and energy-dispersive X-ray spectroscopy. An acceleration voltage of 15 kV was used in SEM. The number of EDS scans was 4, and the scan time was 60 s.

3. Results and Discussion

3.1. Combustion Exothermicity Analysis

Variations in ΔH_r and T_{ad} were calculated for Equations (1) and (2) as a function of their stoichiometric coefficients (x and y) in the range between 0.1 and 1.0 and are presented in Figure 2a,b, respectively. Both reactions were highly energetic with T_{ad} above 2600 K, which justifies self-sustaining combustion. However, due to the dilution effect of pre-added MgO and TiO_2, combustion exothermicity was lowered by increasing the amounts of MgO and TiO_2. There are two major heat-releasing reactions involved in the reaction systems (1) and (2). One is the solid-state reaction of Ti with boron to form TiB_2, with $\Delta H_r = -315.9$ kJ/mol of TiB_2. The other is the magnesiothermic reduction of B_2O_3 to generate boron and MgO, which liberates ΔH_r of 177.2 kJ/mol of MgO [28]. Because Mg is a stronger reducing

agent than Ti, the reduction of B_2O_3 was initiated by Mg. Once combustion started off, a portion of Ti could participate in the reaction with B_2O_3 to produce TiO_2. The reaction of B_2O_3 with Ti is less exothermic than that with Mg and has a lower reaction enthalpy of $\Delta H_r = -108.8$ kJ/mol of TiO_2 [28]. For the synthesis of Mg_2TiO_4 from Reaction (1) under $0.1 \leq x \leq 1.0$, MgO was partly produced from the magnesiothermic reduction of B_2O_3 and partly supplied from pre-added MgO, but TiO_2 was totally generated from the reaction of Ti with B_2O_3. Because Reaction (2) adopts TiO_2-added samples, the sources of MgO and TiO_2 for the formation of Mg_2TiO_4 are opposite to those of Reaction (1). It should be noted that the formation of Mg_2TiO_4 from a solid-state reaction between TiO_2 and MgO is an endothermic process with $\Delta H_r = 302.8$ kJ/mol of Mg_2TiO_4 [28].

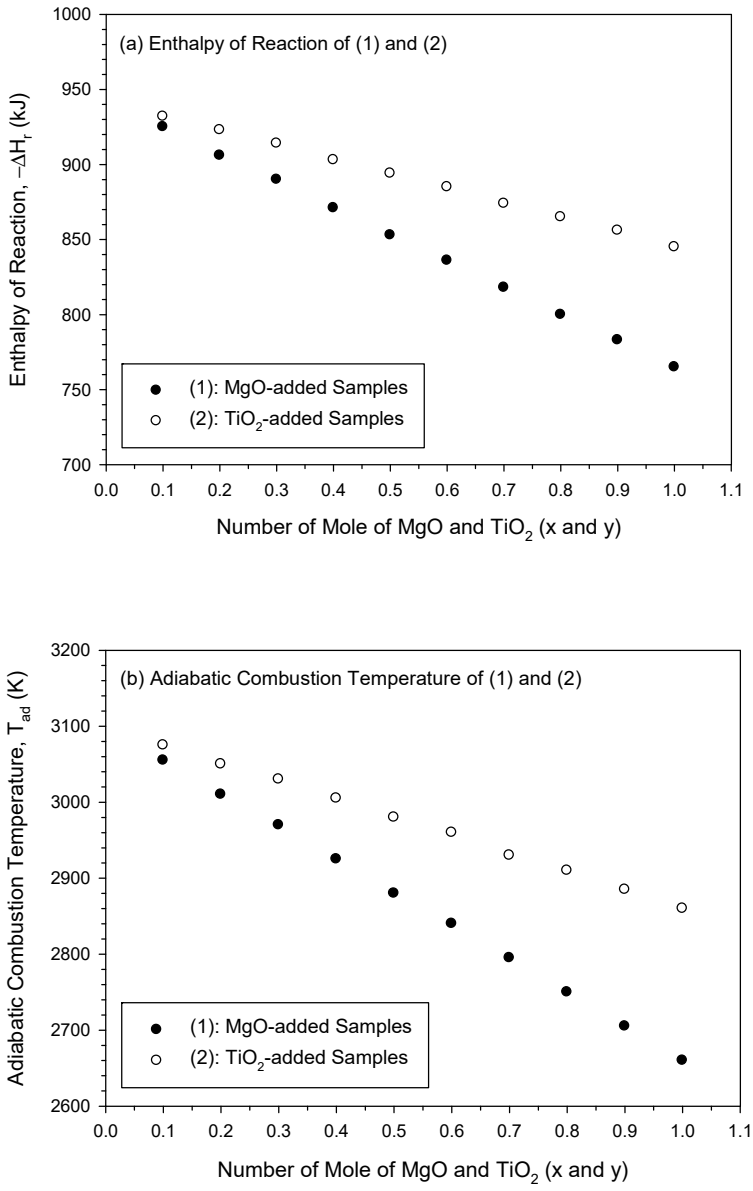

Figure 2. Variations of (**a**) enthalpy of reaction (ΔH_r) and (**b**) adiabatic combustion temperature (T_{ad}) with the number of moles of MgO and TiO_2 for MgO-added samples of the reaction system (1) and TiO_2-added samples of the reaction system (2).

Figure 2a,b shows the decrease in ΔH_r from −925 to −765 kJ for Reaction (1) with increasing MgO content from x = 0.1 to 1.0, within which T_{ad} declines from 3055 to 2660 K. Similarly, as revealed in Figure 2a,b, the increase in TiO_2 from y = 0.1 to 1.0 in Reaction (2) leads to a decrease in both ΔH_r (from −932 to −845 kJ) and T_{ad} (from 3075 to 2860 K). A

more pronounced decrease in both ΔH_r and T_{ad} was observed for Reaction (1), suggesting a stronger dilution effect on combustion imposed by MgO than TiO_2 addition. This was attributed to the fact that the increase in MgO in Reaction (1) decreased the magnitude of the magnesiothermic reduction of B_2O_3. However, the amount of MgO produced from the reduction of B_2O_3 was not affected by the addition of TiO_2 in Reaction (2). That is, the extent of magnesiothermic reduction of B_2O_3 remained unchanged in Reaction (2). As mentioned above, the reduction of B_2O_3 by Mg is more exothermic than the reaction of B_2O_3 with Ti. Moreover, it is noteworthy that the number of moles of MgO required to form Mg_2TiO_4 is twice as many as that of TiO_2.

3.2. Self-Propagating Combustion Wave Kinetics

Two typical time sequences of recorded combustion images are illustrated in Figure 3a,b, which shows the SHS processes of powder compacts of the reaction systems (1) with x = 0.5 and (2) with y = 0.5, respectively. As shown in Figure 3, a scale image was recorded and displayed on the left-hand side of each recorded photo; the scale bar has a unit of 1 mm. It is evident that both combustion processes became self-sustaining upon initiation and featured a distinct combustion front propagating along the powder compact. The combustion of the MgO-added sample shown in Figure 3a appeared to be less violent and took a longer time to complete the flame propagation when compared with that of the TiO_2-containing sample in Figure 3b. This implies a higher exothermicity of Reaction (2) and agrees with thermodynamic calculations. Moreover, the visual observation of recorded films clearly revealed that the degree of combustion strength and the intensity of burning glow were gradually alleviated as the amount of MgO and TiO_2 increased in the samples.

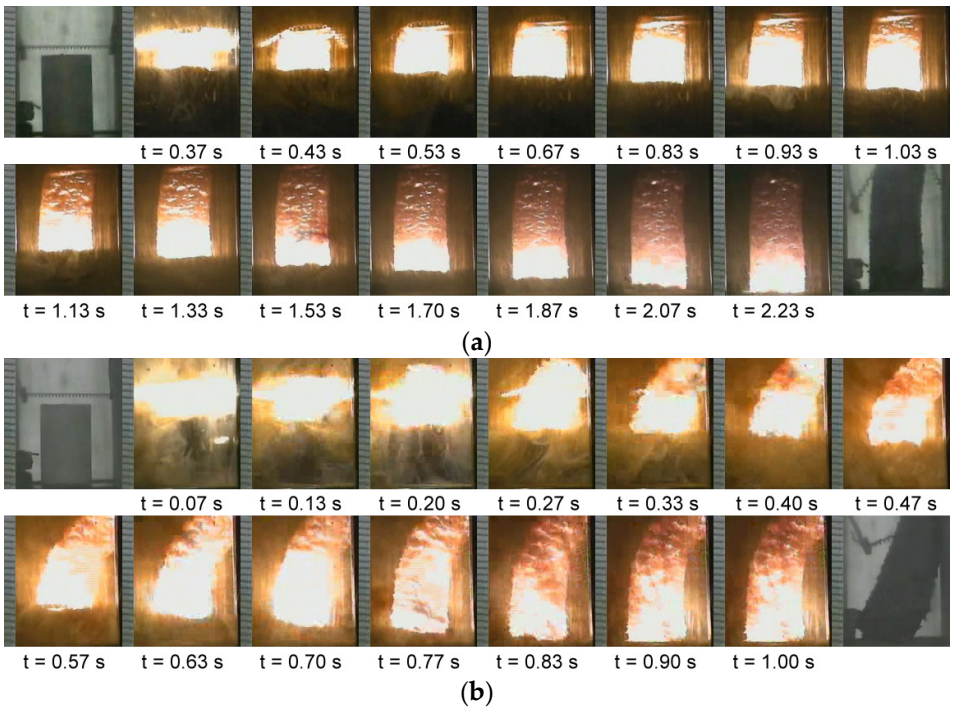

Figure 3. Time sequences of SHS processes with self-sustaining combustion waves recorded from (**a**) MgO-added samples of the reaction system (1) with x = 0.5 and (**b**) TiO_2-added samples of the reaction system (2) with y = 0.5. (Unit of scale bar: 1 mm.)

Figure 4 presents the measured combustion wave velocities (V_f) of the reaction systems (1) and (2) containing different molar contents of pre-added MgO and TiO_2. Figure 3 indicates that for the reaction system (1), as the amount of MgO increases from 0.1 to 1.0 mol, the combustion wave velocity decreases significantly from 8.6 to 2.1 mm/s. The deceleration of the combustion wave resulted largely from the lessening of combustion

exothermicity. Because heat transfer by conduction from the thin reaction zone to its adjacent unburned region plays an important role in establishing a self-sustaining combustion wave, the propagation velocity, in large part, is governed by the reaction zone temperature. For the reaction system (2), the decline in combustion wave spreading speed was relatively moderate, and the flame velocity was lowered from 11 to 7.2 mm/s when the number of moles of TiO_2 increased from 0.1 to 1.0. Not only was the combustion wave velocity of the reaction system (2) higher than that of Reaction (1), but also the discrepancy between them became larger as the amounts of MgO and TiO_2 augmented. The velocity difference between the two reaction systems expanded from about 2.4 to 5.1 mm/s. This indicates that MgO imposes a stronger attenuation effect on combustion, and its influence is more intense as MgO increases.

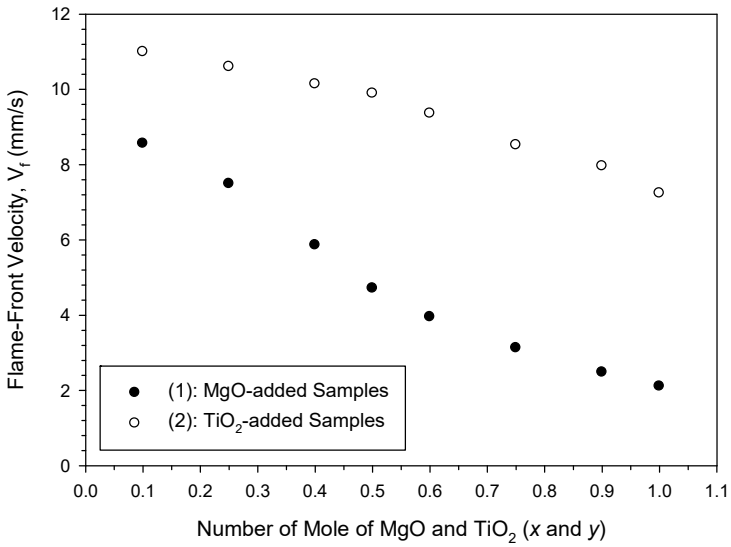

Figure 4. Variations of combustion wave propagation velocities of the reaction systems (1) and (2) with the number of moles of MgO and TiO_2 (i.e., stoichiometric coefficients: x and y).

Three typical combustion temperature profiles are depicted in Figure 5a,b, and they were respectively measured from the powder compacts of the reaction systems (1) and (2) with different MgO and TiO_2 contents. All profiles exhibit a sharp positive gradient, signifying the speedy arrival of the combustion front. Because of a thin reaction zone, the peak value is considered the combustion front temperature (T_c). After the rapid progression of the combustion wave, the profile showed a dramatic temperature decrease, indicating the burned sample was experiencing a rapid cooling rate. The temperature profile is characteristic of the SHS reaction, which features a thin reaction zone and a speedy combustion wave. Three temperature profiles depicted in Figure 5a show T_cs of 1607 °C, 1466 °C, and 1312 °C for the samples of Reaction (1) at x = 0.25, 0.5, and 1.0, respectively. Due to higher exothermicity for Reaction (2), as revealed in Figure 5b, higher T_cs reaching 1658 °C, 1588 °C, and 1467 °C were detected correspondingly for the powder compacts of y = 0.25, 0.5, and 1.0. As expected, the highest combustion front temperatures for the reaction systems (1) and (2) were measured at x = 0.1 and y = 0.1, respectively. The highest T_c of Reaction (1) approached 1670 °C, which is slightly lower than that of Reaction (2) at 1705 °C. It is worth mentioning that the dependence of T_c on the content of MgO and TiO_2 not only validated the thermal analysis calculations but also justified the variation in combustion wave velocity with the stoichiometric coefficient. When compared with the calculated adiabatic temperature T_{ad}, however, the measured combustion front temperature T_c appeared to be much lower. This suggests that combustion of the powder compact was subject to extensive heat losses to the surrounding argon gas by conduction and convection, to the steel sample holder by conduction, and to the chamber inner wall by radiation.

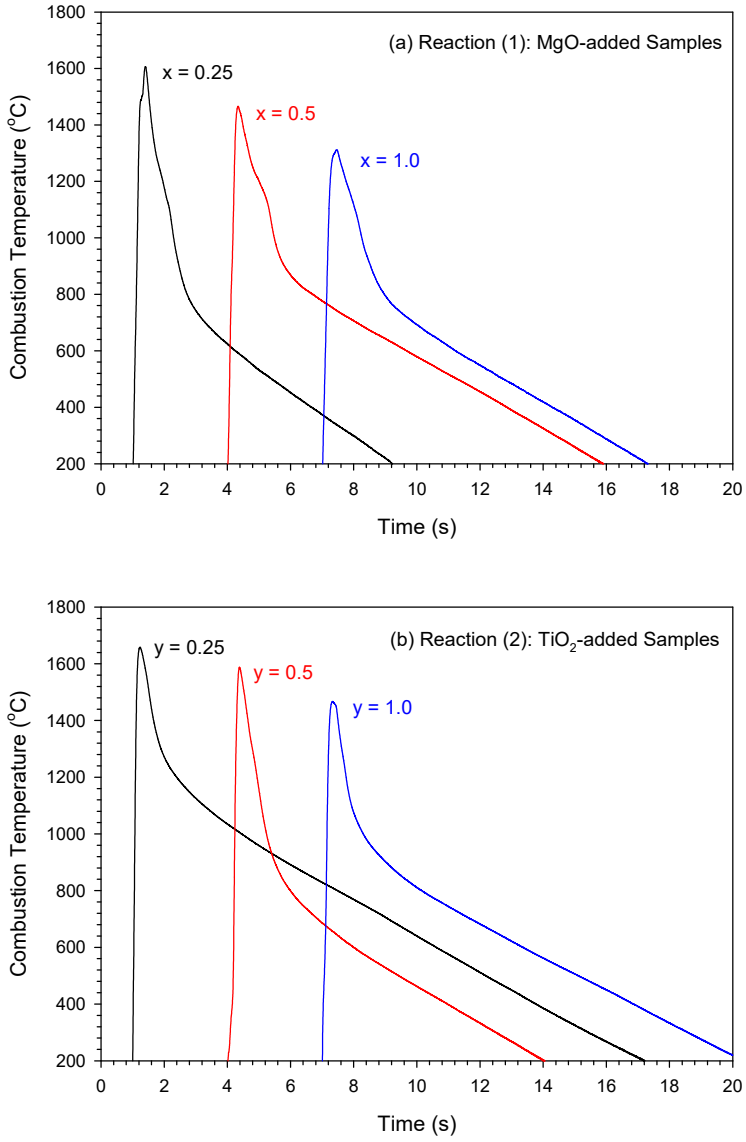

Figure 5. Combustion temperature profiles of (**a**) Reaction (1): MgO-added samples with x = 0.25, 0.5, and 1.0 and (**b**) Reaction (2): TiO_2-added samples with y = 0.25, 0.5, and 1.0.

According to combustion wave kinetics [30], the activation energy (E_a) of a solid-state combustion reaction can be determined from a modified Arrhenius rate equation, as can be seen in Equation (4).

$$V_f{}^2 = \frac{2\lambda}{\rho Q}\frac{RT_c{}^2}{E_a}k_o \exp(-E_a/RT_c) \tag{4}$$

where λ is the thermal conductivity, R is the universal gas constant, Q is the heat of the reaction, and k_o is a constant. The use of experimental data for V_f and T_c to construct the variation in $\ln(V_f/T_c)^2$ with $1/T_c$ has been widely employed to deduce E_a [27,31]. That is, the slope of a linear line correlating $\ln(V_f/T_c)^2$ and $1/T_c$ signifies E_a/R. Figure 6 plots two sets of experimental data for the reaction systems (1) and (2) and their respective best-fitted linear lines and slopes. From the slopes of two straight lines, the activation energies E_a of 183 and 91 kJ/mol were obtained for (1) and (2), respectively. A larger E_a for (1) means a higher kinetic barrier for the synthesis reaction to occur. Because the magnesiothermic reduction of B_2O_3 is considered the initiation step of the SHS process in (1) and (2), the extent of magnesiothermic reduction of (1) is less than that of (2). In addition, the TiO_2 required in (1) must be all produced from the reduction reaction of B_2O_3 by Ti, which is

more difficult to achieve than the magnesiothermic reduction of B_2O_3. On the contrary, (2) contains pre-added TiO_2 and fulfills a complete magnesiothermic reduction. From the thermodynamic point of view, the combustion exothermicity of (2) is greater than that of (1), which also facilitates the reaction to be initiated and carried out.

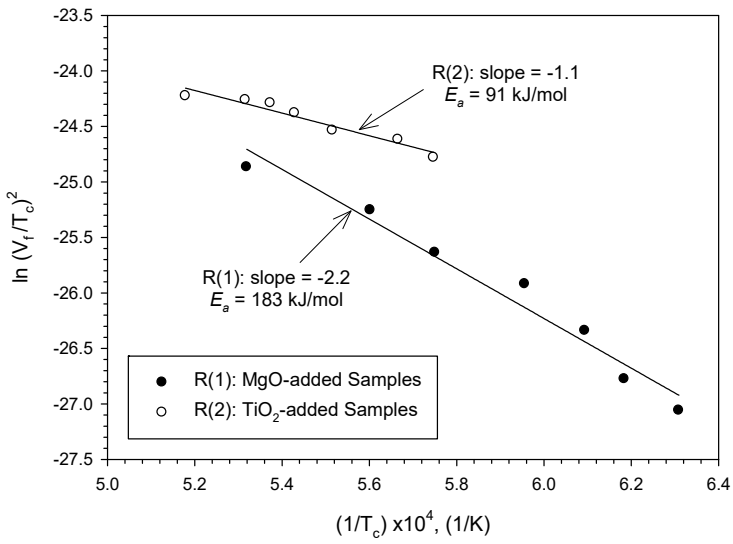

Figure 6. Linear correlation between $\ln(V_f/T_c)^2$ and $1/T_c$ for determination of activation energies (E_a) of reaction systems (1) and (2).

3.3. Phase Composition and Microstructure of Synthesized Products

Figure 7a,b presents typical XRD spectra of TiB_2–Mg_2TiO_4 composites synthesized from the reaction systems (1) with x = 0.5 and (2) with y = 0.5, respectively. In situ formation of TiB_2 and Mg_2TiO_4 from self-sustaining combustion of (1) and (2) under these two conditions was confirmed, and almost no other phases were identified from the XRD analysis. It is believed that the formation of Mg_2TiO_4 was completed by a combination reaction between MgO and TiO_2 during the SHS process. For Reaction (1), MgO was partly from the pre-added precursor and partly from the product of the Mg–B_2O_3 thermite, while TiO_2 was totally generated from the reaction of Ti with B_2O_3. In contrast, the pre-added precursor in Reaction (2) was TiO_2, which reacted with thermite-produced MgO and TiO_2 to form Mg_2TiO_4. Similar to the synthesis of $MgAl_2O_4$ from SHS involving reducing stages [25], the evolution of Mg_2TiO_4 could be governed by a dissolution–precipitation mechanism. Namely, in situ-formed MgO and TiO_2 dissolved into pre-added TiO_2 or MgO particles, and Mg_2TiO_4 grains then precipitated as saturation was achieved.

It should be noted that for the reaction system (1), the XRD pattern of the final products synthesized from the samples of x = 0.9 and 1.0 indicated the presence of a trivial amount of another magnesium titanate, $MgTiO_3$, which was considered an intermediate phase for the formation of Mg_2TiO_4. During the SHS process, it is believed that the reaction of TiO_2 with MgO forms $MgTiO_3$ first, and $MgTiO_3$ subsequently combines with another MgO to become Mg_2TiO_4. Low reaction temperatures of about 1310–1340 °C for (1) with x = 0.9 and 1.0 could be responsible for this incomplete conversion. In contrast, the synthesized products from (2) with y = 0.1–1.0 contained no $MgTiO_3$ and other unwanted phases. This could be attributed to its high reaction temperatures of 1467–1705 °C.

In summary, the formation mechanism of TiB_2–Mg_2TiO_4 composites involves an elemental reaction, a metallothermic reduction, and a combination reaction. For both reaction systems, the initiation step was the magnesiothermic reduction of B_2O_3 to form MgO and boron, as in Reaction (5). Subsequently, the elemental reaction of Ti with boron took place to produce TiB_2, as in Reaction (6). Both Reactions (5) and (6) were highly exothermic, so the reduction of B_2O_3 by Ti, as in Reaction (7), was triggered to form TiO_2

and boron. Next, a series of combination reactions between MgO and TiO_2 occurred as in Reactions (8) and (9), which yielded $MgTiO_3$ and then Mg_2TiO_4.

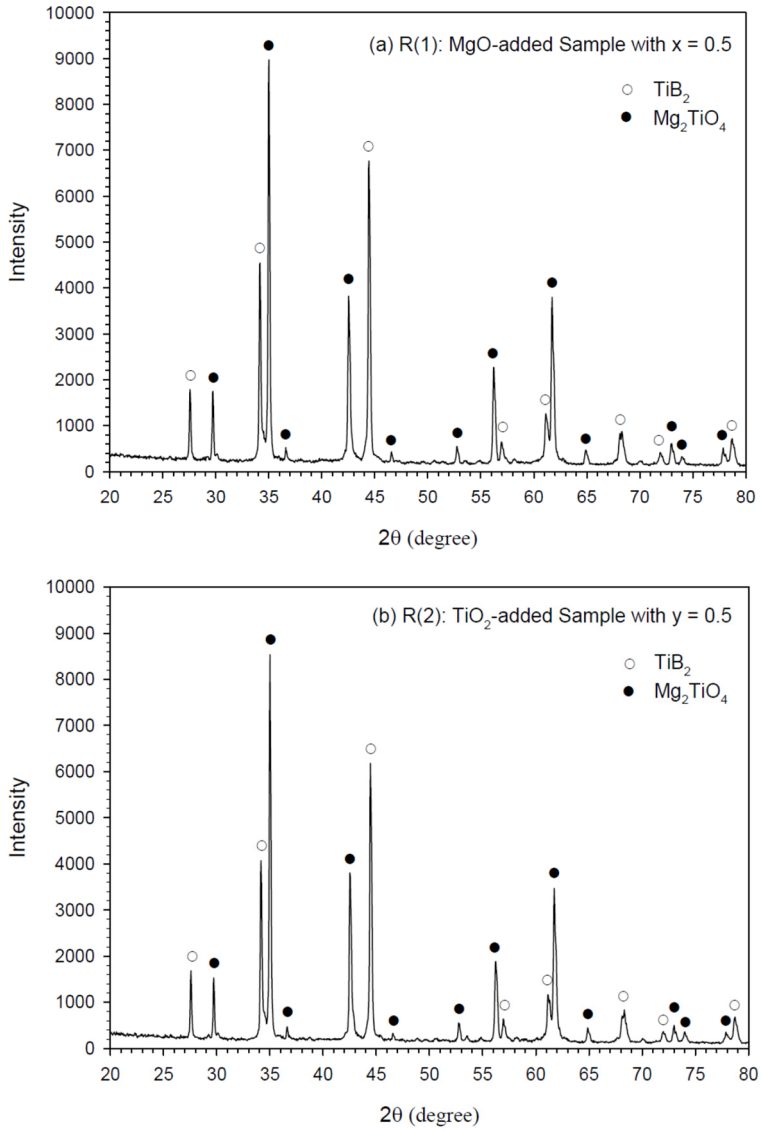

Figure 7. XRD patterns of TiB_2–Mg_2TiO_4 composites synthesized from (**a**) MgO-added samples of the reaction system (1) with x = 0.5 and (**b**) TiO_2-added samples of the reaction system (2) with y = 0.5.

$$\mathrm{Mg} + \frac{1}{3}\mathrm{B_2O_3} \rightarrow \mathrm{MgO} + \frac{2}{3}B \tag{5}$$

$$\mathrm{Ti} + 2\mathrm{B} \rightarrow \mathrm{TiB_2} \tag{6}$$

$$\mathrm{Ti} + \frac{2}{3}\mathrm{B_2O_3} \rightarrow \mathrm{TiO_2} + \frac{4}{3}B \tag{7}$$

$$\mathrm{MgO} + \mathrm{TiO_2} \rightarrow \mathrm{MgTiO_3} \tag{8}$$

$$\mathrm{MgTiO_3} + \mathrm{MgO} \rightarrow \mathrm{Mg_2TiO_4} \tag{9}$$

The samples for the SEM examination were taken from the cross-section surface of the synthesized sample. Figure 8a is the SEM image illustrating the microstructure of the fracture surface of the synthesized product of the reaction system (1) with x = 0.5. The morphology displays uniformly distributed Mg_2TiO_4 agglomerates (the irregular gray chunks) with a size of 3–5 μm. EDS analysis was conducted to identify Mg_2TiO_4 and TiB_2

from the SEM images. The locations of point analysis on the SEM images were indicated with an x sign; that is, P1 and P2 are pointed out in Figure 8a and P3 and P4 in Figure 8b. An atomic ratio of Mg:Ti:O = 26.7:15.2:58.1, which is close to the stoichiometry of Mg_2TiO_4, was detected for the agglomerates based on the EDS analysis at P1. TiB_2 crystals (the small white grains), which were confirmed by an atomic ratio of Ti:B = 32.4:67.6 at P2, existed in the interstices among Mg_2TiO_4 grains. TiB_2 crystals were formed as either short rods with a length of 1–2 μm or flattened platelets with a thickness of 0.5–1.0 μm. The final products of (1) all exhibited a similar microstructure to Figure 8a. For the TiB_2–Mg_2TiO_4 composite obtained from the reaction system (2), Figure 8b also unveils a similar microstructure to that shown in Figure 8a. Small TiB_2 crystals in the shape of short rods and thin platelets were present within the gaps of Mg_2AlO_4 grains. Both phases were well distributed and closely packed. For the Mg_2TiO_4 and TiB_2 grains in Figure 8b, elemental ratios of Mg:Ti:O = 29.1:13.8:57.1 and Ti:B = 34.6:65.4 were obtained by the EDS analysis at P3 and P4, respectively.

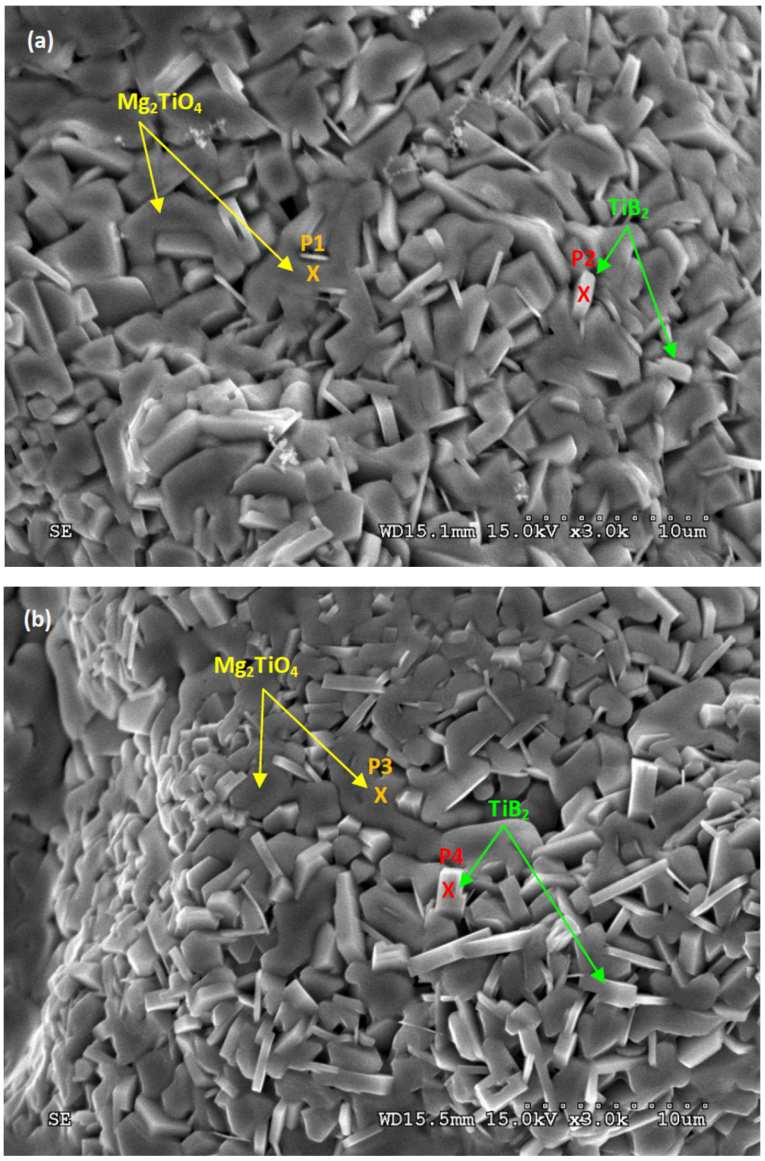

Figure 8. SEM micrographs of TiB_2–Mg_2TiO_4 composites synthesized from (**a**) MgO-added samples of the reaction system (1) with x = 0.5 and (**b**) TiO_2-added samples of the reaction system (2) with y = 0.5.

4. Conclusions

In situ formation of TiB_2–Mg_2TiO_4 composites with a molar ratio of TiB_2:Mg_2TiO_4 = 1.5:1 was completed by combustion synthesis integrating magnesiothermic reduction of B_2O_3 with a solid-state reaction between Ti and boron. Two types of green mixtures were considered: one adopted MgO as the combustion moderator and a part of the precursor of Mg_2TiO_4; the other employed TiO_2. The amounts of pre-added MgO and TiO_2 were varied within 0.1 to 1.0 mol to ensure combustion of both types of sample compacts was stable and sufficiently exothermic to take place in the SHS mode. A novel and rapid synthesis route for producing Mg_2TiO_4-containing composites was demonstrated.

According to the analysis of reaction exothermicity, combustion of the MgO-added sample is less energetic than that of the TiO_2-added sample. Experimental results were consistent with the calculations and indicated that the increase in pre-added MgO decreased the combustion front temperature from 1670 to 1312 °C, as well as the combustion wave velocity from 8.6 to 2.1 mm/s. Likewise, a decrease in combustion temperature from 1705 to 1467 °C and flame-front velocity from 11 to 7.2 mm/s was observed for the TiO_2-added samples. MgO was shown to have a greater dilution effect on combustion than TiO_2, because pre-added MgO reduced the extent of magnesiothermic reduction of B_2O_3 in the SHS process. Activation energies E_a of 183 and 91 kJ/mol were deduced for MgO- and TiO_2-added reaction systems, respectively, based on a modified Arrhenius rate equation with measured combustion wave velocities and temperatures. A larger E_a implies a higher kinetic barrier for MgO-added samples to be initiated and proceed because of the reduction of B_2O_3 by both Mg and Ti and low combustion exothermicity. The XRD analysis confirmed in situ formation of the TiB_2–Mg_2TiO_4 composite with almost no other minor phases. It is considered that in the course of the SHS process, Mg_2TiO_4 was produced from the interaction between MgO and TiO_2, both of which were totally or partially generated from the metallothermic reduction of B_2O_3. The dissolution of in situ-formed MgO and TiO_2 into pre-added TiO_2 or MgO particles led to the precipitation of Mg_2TiO_4 grains. The microstructure of the synthesized products based on SEM observations exhibited that two constituent components, TiB_2 and Mg_2TiO_4, were well distributed and closely engaged. Mg_2TiO_4 agglomerates have a size of 3–5 μm. TiB_2 crystals are in the form of short rods of 1–2 μm in length and thin platelets of 0.5–1.0 μm in thickness.

Author Contributions: Conceptualization, C.-L.Y.; validation, C.-L.Y. and C.C.; methodology, C.-L.Y. and C.C.; data curation, C.-L.Y. and C.C.; formal analysis, C.-L.Y. and C.C.; resources, C.-L.Y.; investigation, C.-L.Y. and C.C.; writing—original draft preparation, C.-L.Y. and C.C.; writing—review and editing, C.-L.Y. and C.C.; project administration, C.-L.Y.; supervision, C.-L.Y.; funding acquisition, C.-L.Y. All authors have read and agreed to the published version of the manuscript.

Funding: This research was funded by the National Science and Technology Council of Taiwan, and the grant number was NSTC 112-2221-E-035-041-MY2.

Data Availability Statement: The data presented in this study are available in the article.

Conflicts of Interest: The authors declare no conflicts of interest.

References

1. Binner, J.; Porter, M.; Baker, B.; Zou, J.; Venkatachalam, V.; Diaz, V.R.; D'Angio, A.; Ramanujam, P.; Zhang, T.; Murthy, T.S.R.C. Selection, processing, properties and applications of ultra-high temperature ceramic matrix composites, UHTCMCs—A review. *Int. Mater. Rev.* **2020**, *65*, 389–444. [CrossRef]
2. Yurkov, A. Silicon carbide–silicon nitride refractory materials: Part 1 materials science and processing. *Processes* **2023**, *11*, 2134. [CrossRef]
3. Golla, B.R.; Mukhopadhyay, A.; Basu, B.; Thimmappa, S.K. Review on ultra-high temperature boride ceramics. *Prog. Mater. Sci.* **2020**, *111*, 100651. [CrossRef]
4. Basu, B.; Raju, G.B.; Suri, A.K. Processing and properties of monolithic TiB_2 based materials. *Int. Mater. Rev.* **2006**, *51*, 352–374. [CrossRef]
5. Königshofer, R.; Fürnsinn, S.; Steinkellner, P.; Lengauer, W.; Haas, R.; Rabitsch, K.; Scheerer, M. Solid-state properties of hot-pressed TiB_2 ceramics. *Int. J. Refract. Met. Hard Mater.* **2005**, *23*, 350–357. [CrossRef]

6. Parlakyigit, A.S.; Ergun, C. A facile synthesis method for in situ composites of TiB_2/B_4C and ZrB_2/B_4C. *J. Aust. Ceram. Soc.* **2022**, *58*, 411–420. [CrossRef]
7. Liu, X.; Luo, H.; Yang, J.; Wang, X.; Qu, Z.; Luo, H.; Gong, R. Enhancement on high-temperature microwave absorption properties of TiB_2–MgO composites with multi-interfacial effects. *Ceram. Int.* **2021**, *47*, 4475–4485. [CrossRef]
8. Zhao, S.; Ma, H.; Shao, T.; Wang, J.; Zhang, L.; Sui, S.; Feng, M.; Wang, J.; Qu, S. Thermally stable ultra-thin and refractory microwave absorbing coating. *Ceram. Int.* **2021**, *47*, 17337–17344. [CrossRef]
9. Zhang, Q.; Chen, T.; Kang, W.; Xing, X.; Wu, S.; Gou, Y. Synthesis of Polytitanocarbosilane and Preparation of Si–C–Ti–B Fibers. *Processes* **2023**, *11*, 1189. [CrossRef]
10. Shen, S.; Song, S.; Wang, J.; Li, R.; Li, X.; Zhen, Q. Anisotropic binary TiB_2–SiC composite powders: Synthesis and microwave absorption properties. *Ceram. Int.* **2022**, *48*, 8579–8588. [CrossRef]
11. Yang, J.; Liu, X.; Gong, W.; Wang, T.; Wang, X.; Gong, R. Temperature-insensitive and enhanced microwave absorption of $TiB_2/Al_2O_3/MgAl_2O_4$ composites: Design, fabrication, and characterization. *J. Alloys Compd.* **2022**, *894*, 162144. [CrossRef]
12. Kumar, S.; Kumar, R.; Koo, B.H.; Choi, H.; Kim, D.U.; Lee, C.G. Structural and electrical properties of Mg_2TiO_4. *J. Ceram. Soc. Jpn.* **2009**, *117*, 689–692. [CrossRef]
13. Li, H.; Xiang, R.; Chen, X.; Hua, H.; Yu, S.; Tang, B.; Chen, G.; Zhang, S. Intrinsic dielectric behavior of Mg_2TiO_4 spinel ceramic. *Ceram. Int.* **2020**, *46*, 4235–4239. [CrossRef]
14. Cheng, L.; Liu, P.; Qu, S.X.; Cheng, L.; Zhang, H. Microwave dielectric properties of Mg_2TiO_4 ceramics synthesized via high energy ball milling method. *J. Alloys Compd.* **2015**, *623*, 238–242. [CrossRef]
15. Hu, Q.; Teng, Y.; Zhao, X.; Arslanov, T.; Zheng, Q.; Luo, T.; Ahuja, R. Temperature stable dielectric properties of Mg_2TiO_4–$MgTiO_3$–$CaTiO_3$ ceramics over a wide temperature range. *Ceram. Int.* **2023**, *49*, 1997–2006. [CrossRef]
16. Hamzawy, E.M.; Margha, F.H.; Morsi, R.M. Crystallization and electrical measurements of sintered qandilite (Mg_2TiO_4)-borosilicate glass composite. *J. Aust. Ceram. Soc.* **2023**, *59*, 281–290. [CrossRef]
17. Belous, A.; Ovchar, O.; Durilin, D.; Krzmanc, M.M.; Valant, M.; Suvorov, D. High-Q microwave dielectric materials based on the spinel Mg_2TiO_4. *J. Am. Ceram. Soc.* **2006**, *89*, 3441–3445. [CrossRef]
18. Yang, X.; Lai, Y.; Zeng, Y.; Yang, F.; Huang, F.; Li, B.; Wang, F.; Wu, C.; Su, H. Spinel-type solid solution ceramic $MgAl_2O_4$–Mg_2TiO_4 with excellent microwave dielectric properties. *J. Alloys Compd.* **2022**, *898*, 162905. [CrossRef]
19. Zhang, J.; Shen, B.; Zhai, J.; Yao, X. Microwave dielectric properties and low sintering temperature of $Ba_{0.5}Sr_{0.5}TiO_3$–Mg_2TiO_4 composites synthesized in situ by the hydrothermal method. *Ceram. Int.* **2013**, *39*, 5943–5948. [CrossRef]
20. Xu, J.; Ma, P.; Zou, B.; Yang, X. Reaction behavior and formation mechanism of ZrB_2 and ZrC from the Ni-Zr-B_4C system during self-propagating high-temperature synthesis. *Materials* **2023**, *16*, 354. [CrossRef] [PubMed]
21. Levashov, E.A.; Mukasyan, A.S.; Rogachev, A.S.; Shtansky, D.V. Self-propagating high-temperature synthesis of advanced materials and coatings. *Int. Mater. Rev.* **2017**, *62*, 203–239. [CrossRef]
22. Amiri-Moghaddam, A.; Kalantar, M.; Hasani, S. Synthesis of Al_2O_3-WSi_2-WB_2-WB composite in Al-Si-WO_3-B_2O_3 system by self-propagating high-temperature synthesis. *J. Aust. Ceram. Soc.* **2022**, *58*, 1157–1165. [CrossRef]
23. Yeh, C.L.; Li, R.F. Formation of TiB_2-Al_2O_3 and NbB_2-Al_2O_3 composites by combustion synthesis involving thermite reactions. *Chem. Eng. J.* **2009**, *147*, 405–411. [CrossRef]
24. Zaki, Z.I.; Mostafa, N.Y.; Rashad, M.M. High pressure synthesis of magnesium aluminate composites with $MoSi_2$ and Mo_5Si_3 in a self-sustaining manner. *Ceram. Int.* **2012**, *38*, 5231–5237. [CrossRef]
25. Yeh, C.L.; Chen, M.C.; Shieh, T.H. Formation of silicide/spinel ceramic composites via Al- and Mg-based thermitic combustion synthesis. *J. Aust. Ceram. Soc.* **2022**, *58*, 1275–1282. [CrossRef]
26. Zaki, Z.I.; Ahmed, Y.M.Z.; Abdel-Gawad, S.R. In-situ synthesis of porous magnesia spinel/TiB_2 composite by combustion technique. *J. Ceram. Soc. Jpn.* **2009**, *117*, 719–723. [CrossRef]
27. Yeh, C.L.; Zheng, F.Y. Formation of TiB_2-$MgAl_2O_4$ composites by SHS metallurgy. *Materials* **2023**, *16*, 1615. [CrossRef]
28. Binnewies, M.; Milke, E. *Thermochemical Data of Elements and Compounds*; Wiley-VCH Verlag GmbH: Weinheim, Germany, 2002.
29. Yeh, C.L.; Chen, Y.L. An experimental study on self-propagating high-temperature synthesis in the Ta-B_4C system. *J. Alloys Compd.* **2009**, *478*, 163–167. [CrossRef]
30. Varma, A.; Rogachev, A.S.; Mukasyan, A.S.; Hwang, S. Combustion synthesis of advanced materials: Principals and applications. *Adv. Chem. Eng.* **1998**, *24*, 79–225.
31. Yeh, C.L.; Chen, K.T. Fabrication of FeSi/α-$FeSi_2$–based composites by metallothermically assisted combustion synthesis. *J. Aust. Ceram. Soc.* **2021**, *57*, 1415–1424. [CrossRef]